Comparison of Photoluminescence Quantum Yield of Single Gold Nanobipyramids and Gold Nanorods

Wenye Rao, Qiang Li, Yuanzhao Wang, Tao Li, and Lijun Wu*

Guangdong Provincial Key Laboratory of Nanophotonic Functional Materials and Devices, School of Information and Optoelectronic Science and Engineering, South China Normal University, Guangzhou 510006, P.R. China

ABSTRACT Fluorescent gold nanoparticles with high quantum yield are highly desirable for optical imaging in the fields of biology and materials science. We investigate the one-photon photoluminescence (PL) properties of individual gold nanobipyramids (GNBs) and find they are analogous to those of the extensively studied gold nanorods (GNRs). By combining PL and atomic force microscopy (AFM) measurements with discrete dipole approximation (DDA) simulations, we obtain the PL quantum yield of single GNRs and GNBs. Compared to GNRs in the similar surface plasmon resonance range, the PL quantum yield of GNBs is found to be doubled. The stronger field intensity around GNBs can explain their higher PL quantum yields. Our research would provide deeper understanding of the mechanism of PL from gold nanoparticles as well as be beneficial for finding out optical imaging labels with high contrast.

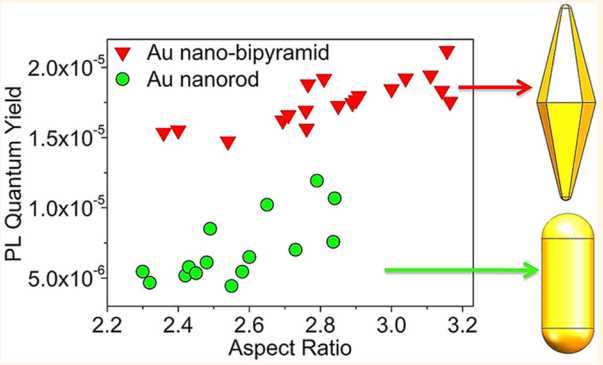

KEYWORDS: gold nanobipyramids · gold nanorods · photolumincence · surface plasmon resonance · quantum yield

Localized surface plasmon polaritons (LSPPs) or surface plasmon resonances (SPRs) excited in noble metallic nanoparticles have attracted great interest in the past decade due to their potential applications in various fields of nanometer science and technology.[1] The collective oscillation of their free electrons giving rise to large scattering and absorption cross section have been widely investigated and applied to many applications.[2,3] Recently, the photoluminescence (PL) from gold nanoparticles has proven to be a complementary property to absorption and scattering for imaging and sensing purposes.[4−7] For example, the PL from gold nanocubes have been successfully applied in cell imaging of human liver cancer cells[8] and gold nanorods (GNRs) have been utilized as orientation sensors by defocused imaging their single-photon PL.[9]

PL from noble metals was first reported in 1969 by Mooradian.[10] Since the spectrum did not depend on the excitation wavelength, the origin was not assigned to Raman scattering but to luminescence. This luminescence was originally described as a three-step process. (1) The direct absorption of photons at the excitation promotes electrons from energy bands below the Fermi level into bands above it. (2) After absorption, the electrons and holes rapidly relax toward the Fermi level *via* electron−electron and electron−phonon scattering processes. (3) The luminescence then results from the low probability of radiative recombination of these relaxing electron−hole pairs.[10−14] The PL quantum yield (QY) of bulk gold is as low as on the order of 10^{-10}.[10] It was found that rough surfaces can improve the PL QY of metals to be several orders of magnitude higher.[11,12] Boyd *et al.* suggested that the local field enhancement plays a dominate role on increasing the PL from metals.[11] This was then named as "lightning-rod effect" (at sharp angled surfaces)[12] and applied to understanding the PL enhancement in gold nanoparticles.[12,13] With the increase of the PL QY from gold nanoparticles, a plasmon emission mechanism was proposed to explain the PL enhancement.[15] It suggests that the

* Address correspondence to ljwu@scnu.edu.cn.

Received for review November 24, 2014 and accepted February 9, 2015.

Published online February 09, 2015
10.1021/nn506689b

energy from the recombination of electron−hole pairs in the third step of the luminescence process is transferred to a plasmon excitation, which then emits a photon. However, no conclusive mechanism has been obtained yet.

Early experiments to understand the mechanism of the emission have relied on ensemble measurements.[12,16] Although the enhanced PL QY of gold nanoparticles is still several orders of magnitude lower than that of organic dyes or quantum dots, their large absorption cross section can compensates for this drawback.[9] Furthermore, without time-dependent fluorescence fluctuations (photoblinking) and limited lifetime due to irreversible photochemical changes (photobleaching), they can be attractive alternative labels for imaging applications.[17,18]

Among all the gold nanoparticles, gold nanorod (GNR) possessing special anisotropic structure is the most studied and interesting one because of its strong and unique scattering,[19] absorption,[20] and PL[21] properties. Very recently, based on single-particle measurements, Yorulmaz *et al.* studied the PL QY of single gold nanospheres and GNRs with different aspect ratios and volumes. They observed an increase of QY by about an order of magnitude for GNRs especially when the plasmon resonance wavelength is longer than 650 nm.[22] Their results are reliable because the volume effect on the PL intensity of GNR was eliminated by photothermal signal measurements. To further extend potential applications of gold nanoparticles for optical imaging in the fields of biology and materials science, increasing their PL QY is essential.

On the basis of the shape of GNR, if we can increase the lightning-rod effect with more sharp tips or edges, the PL QY might be dramatically improved.[8,13] A gold nanobipyramid (GNB) consisting of two pentagonal pyramids with base joined seems to be a suitable candidate. Owing to their special geometric shape, easy fabrication and strong field concentration at their tips, they have been applied in biosensing,[23] and surface-enhanced Raman spectroscopy (SERS) detection *etc.*[24] However, there is no paper investigating the PL QY of GNBs and only a few studies have investigated their PL properties.[25]

Here, by tuning the polarization in the incident and output optical circuits, we present a detailed study of the PL and scattering properties of GNBs based on single-particle measurements. We compare them with those of GNRs and try to understand the radiating mechanism of GNBs. On the other hand, we correlate atomic force microscopy (AFM) and PL measurements on single GNBs and GNRs and investigate their PL QYs with different sizes and aspect ratios. As is known, AFM can only measure the height precisely due to a convolution effect.[26] We thus measure the height of the monitored GNB/GNR and take their corresponding PL spectra. When we combine their heights and positions

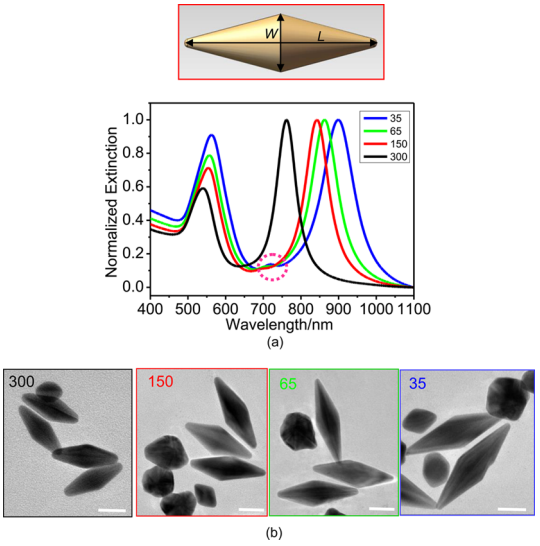

Figure 1. (a) Ensemble extinction spectra of GNBs taken in aqueous solutions with average aspect ratios of 2.5 (seed volume 300 μL), 2.7 (seed volume 150 μL), 2.9 (seed volume 65 μL), and 3.5 (seed volume 35 μL). (b) Corresponding representative TEM images of GNBs. The scale bar dimension is 50 nm. By statistically analyzing all the TEM results, the apex angles between the extended side edge lines are found to be 33.2° ± 1.5°, 31.9° ± 1.7°, 31° ± 1.5°, and 29.2° ± 1.8° for the samples fabricated with the seed volume 300, 150, 65, and 35 μL, respectively. The first angle represents the averaged value and the second one the offset. The top inset plots the schematic of a GNB, in which *W* represents the width, *L* the length and *L*/*W* the aspect ratio.

of SPR in the PL spectra, the aspect ratio and the effective volume value can be calculated out by discrete dipole approximation (DDA) simulations. In this way, the volume effect can be eliminated and the measured PL QY is relatively precise. To the best of our knowledge, this is the first demonstration of comparing the PL QY of GNRs and GNBs at a single-particle level. After calculating and integrating the field intensity over the volume surrounding individual GNBs and GNRs, respectively, we find that the improved PL QY can be ascribed to the strong field enhancement. Our investigations would provide deeper understanding of the mechanism of PL from gold nanoparticles. This study will be beneficial for finding out optical imaging labels with high contrast in the fields of biology and materials science.

RESULTS AND DISCUSSION

GNBs and GNRs were both prepared chemically in aqueous solutions by a seed-mediated method.[27−31] The menu for fabricating GNRs is described in the Supporting Information. To synthesize different sized GNBs, the seed amount added to the growth solution was tuned (35, 65, 150, and 300 μL), allowing the production of elongated nanobipyramid with different aspect ratios. Figure 1a illustrates the normalized UV−vis extinction spectra of the fabricated GNBs which exhibit two clearly distinct peaks. The peak around 550 nm is attributed to a combination of

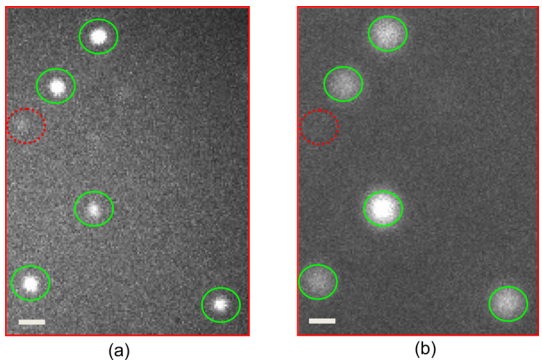

Figure 2. (a) PL image of GNBs. (b) Corresponding DF scattering image. The scale bar dimension is 2 μm.

interband transitions, transverse plasmon resonances from the bases of GNBs and byproduct spherical particles. The other peak at longer wavelength corresponds to the longitudinal plasmon resonance of GNBs. With an increase of the seed volume, the aspect ratio *L*/*W*, which is defined at the top of Figure 1, and the size of the byproduct nanoparticles were all decreased.[29] Thus, both the transverse and longitudinal plasmon resonances blue shift while the longitudinal one is much more distinct because of its high sensitivity to the aspect ratio.[28,29] Compared to the extinction spectra of ensemble GNRs as shown in Supporting Information Figure S1a, the longitudinal plasmon band of GNBs is narrower, which is due to their narrower size distribution during fabrication.[28] Noteworthy is that when the seed volume is decreased to be 65 μL, a small peak positioned by a dashed magenta circle at a wavelength shorter than the longitudinal plasmon band appears, which may be a higher order SPR mode. Figure 1b and Supporting Information Figure S1b show the corresponding transmission electron microscopy (TEM, JEM-2100HR) images. By analyzing the TEM results, the average aspect ratios of GNBs were estimated to be 2.5, 2.7, 2.9, and 3.5, respectively, which were confirmed by DDA simulations through fitting the experimentally measured extinction spectra.

The details for our optical experimental setup are similar to what is shown in our previous papers[9] and schematically plotted in Supporting Information Figure S2. We add a dark-field (DF) scattering measurement here.

Single-particle imaging and spectroscopy are essential to exclude ensemble effects and remove the heterogeneity in the sample. We deposited the fabricated GNBs and GNRs on 0.2 mm thick cleaned glass coverslips at a very low concentration (the coverage is less than 1 rod per μm^2). It was found that GNBs are much easier to separate from each other than GNRs. Figure 2a shows a typical PL image of several individual GNBs, while Figure 2b is the corresponding DF scattering image on the same area. The PL was excited by a 532 nm CW laser. Normally, more GNBs or GNRs can be resolved by PL imaging than by DF scattering imaging on the same microscope. For example, there is one GNB in the PL image (circled by red dotted line) that cannot be resolved by the DF scattering measurement in Figure 2. The higher sensitivity for PL imaging is mainly because the excitation laser could be focused to a diffraction-limited spot which leads to a better spatial resolution. Another point we can observe from Figure 2 is that a brighter GNB shown in the scattering image does not definitely correspond to a brighter spot in the PL image. This can be attributed to the polarization difference of the excitation. In our system, the excitation for PL is linearly polarized. When the long axis of the GNB is noncollinear with the polarization, the excitation would not be efficient. In the case of scattering, the excitation is unpolarized and unrelated with the direction of the GNBs. Therefore, the brightness in the scattering image can disclose the size of single GNBs more directly in our measurements.

Figure 3a demonstrates four typical PL spectra and their corresponding scattering spectra for individual GNBs. Obviously, the longitudinal plasmon resonance in the PL spectrum resemble closely with its scattering spectrum independent of the aspect ratio. As shown in Figure 3b, a typical longitudinal resonance spectrum can be perfectly fitted by a Lorentz function (blue line), revealing that the PL is really from a single GNB.[22] We note that there is a slight difference between the PL and scattering spectra both in terms of peak position and line-shape. This difference has also been observed in gold spheres, disks and nanorods, which was attributed either to higher availability of excited electrons closer to the initial energy of the laser excitation, or to dynamic and photoinduced charging processes.[32,33] However, the underlying mechanism needs to be further investigated.

The polar plot for scattering and PL intensity integrated under the whole spectrum as a function of the excitation and detection polarization are plotted in Figure 3c–f. As can be seen evidently in Figure 3c,e, both the PL and scattering intensity *versus* the excitation polarization exhibit dipolar behavior. In addition, the emission and absorption dipole is collinear not only for PL (refer to Figure 3c,d) but also for scattering (refer to Figure 3e,f). To correlate the PL polarization properties of the GNB with its geometric shape, we scanned its surface morphology by AFM *in situ* and measured its PL intensity under different detection polarization. The results are displayed in Supporting Information Figure S3b. Those for GNR in Supporting Information Figure S3a demonstrate that the relationship is similar, *i.e.*, the PL polarizations are both mainly along the long axis of the GNB and GNR. One thing we have to point out is that we cannot resolve the polarization characterization of the transverse mode in our measurement system because the PL shorter than 550 nm is cut by the dichroscope.

Furthermore, by measuring the PL intensity under different excitation power, the relationship between

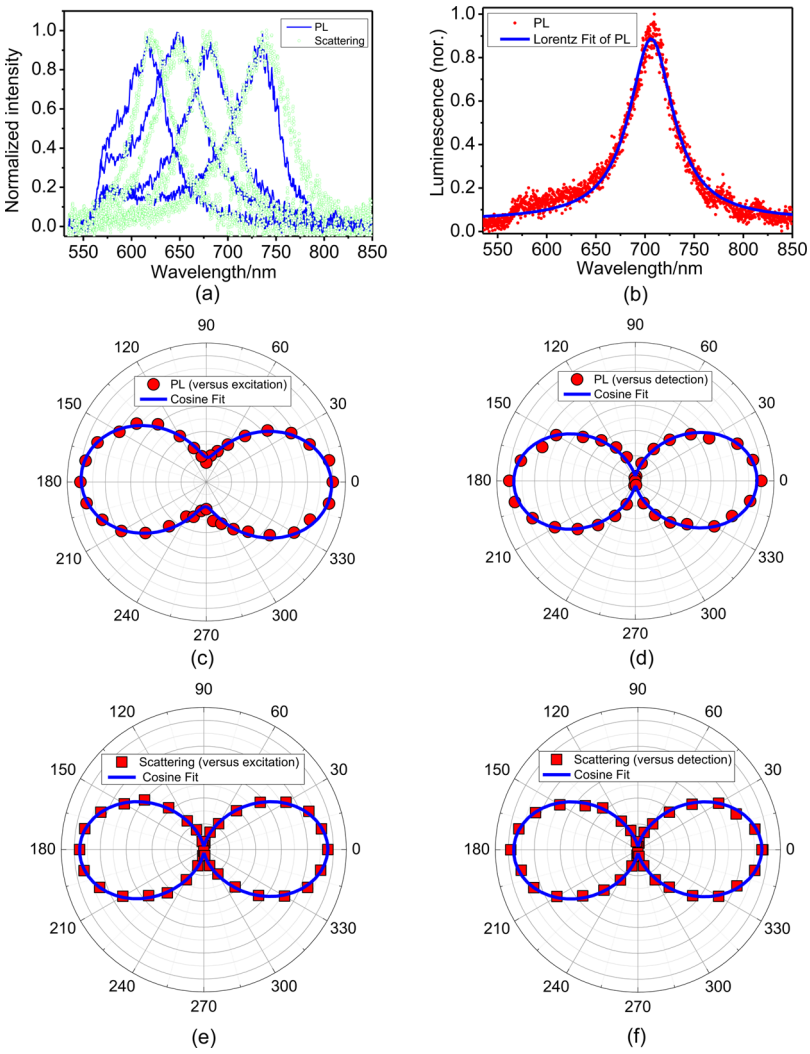

Figure 3. (a) PL (blue solid line) and DF scattering (green open circles) spectra of single GNBs. Please note that the PL shorter than 550 nm was blocked by the dichroic mirror. (b) A typical PL spectrum (red dots) from a GNB can be perfectly fitted by a Lorentz function (blue solid line). (c and d) The polar plot of PL intensity integrated under the whole spectrum (red solid circles) *versus* the excitation/detection polarization direction. (e and f) The polar plot of scattering intensity integrated under the whole spectrum (red solid squares) *versus* the excitation/detection polarization direction. The blue curves are drawn according to the best-fitted cosine functions. In (c) and (d), there was no polarizer in the detection path, while in (d) and (f), the excitation was polarized along the long axis of the GNB.

them was found to be linear, which can be observed obviously in Figure 4. This confirms that the PL from GNBs under a CW excitation at 532 nm is due to a one-photon process.

Summarizing the experimental results shown in Figures 2–4, we can find that they are analogous to those that have been reported for GNRs.[22,33,34] This suggests that the PL from GNBs originates from the similar mechanism as that reported for GNRs.[15,22,33,34]

The reported PL QY of single gold nanoparticles ranges from 10^{-7} to 10^{-4}, depending on several parameters such as size,[8,35,36] fabrication method[12,22], shape[8,22] *etc.* Among them, the shape is one of the most important factors to determine their PL QY. For example, by slowly reshaping a single GNR to a sphere, Yorulmaz *et al.* confirmed that GNRs own a higher PL QY than gold nanospheres because of the lightning-rod

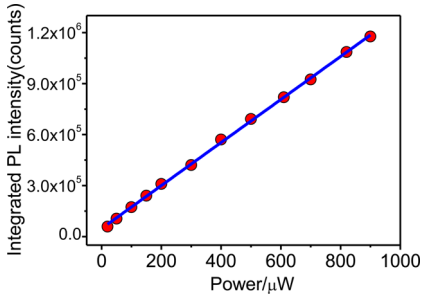

Figure 4. Relationship between the PL intensity integrated under the whole spectrum from a single GNB and the excitation power (532 nm, CW laser). The linear relationship confirms that the PL from GNBs is due to one-photon excitation.

effect.[22] When we compare the geometric shape of GNBs and GNRs shown in Figure 1b and Supporting

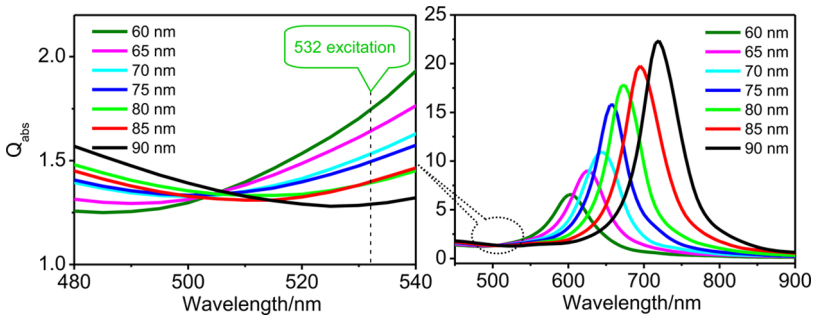

Figure 5. Calculated spectra of the absorption efficiency (Q_{abs}) for GNBs with the diameter fixed at 25 nm and lengths given by the legend. The excitation is along the long axis of GNBs.

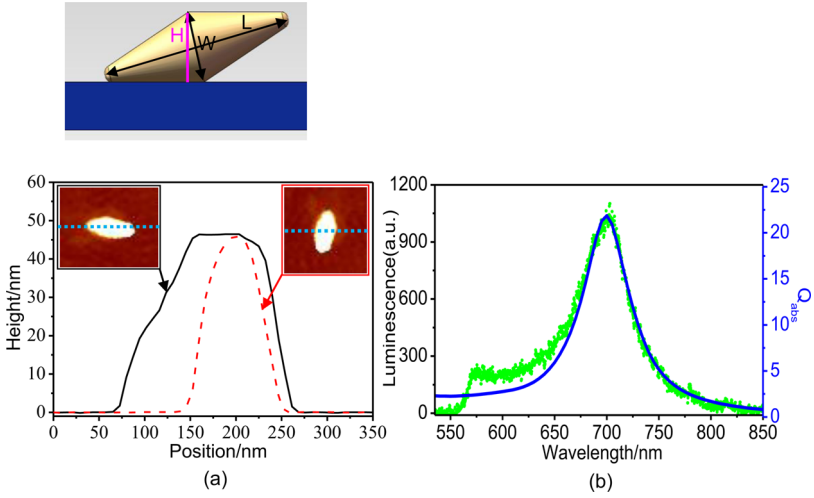

Figure 6. (a) Surface height profile along the long (dark solid line) and short axis (red dashed line) as shown in the AFM images of the target GNB. On the top is the schematic of the GNB sitting on the substrate. (b) Corresponding PL spectrum (green circles) from the target GNB. The blue solid line plots its corresponding simulated absorption spectrum, from which the length *L* of the GNB can be deduced.

Information Figure S1b, the two apexes of GNBs are obviously sharper than those for GNRs, which is supposed to lead to a more remarkable lightning-rod effect. However, to the best of our knowledge, there has been no research work conducted at a single-particle level to confirm this point experimentally. Here, we propose a new method to measure and compare the PL QY of single GNBs and GNRs.

The PL was excited at a wavelength of 532 nm. The PL intensity may be related with the wavelength difference between the excitation and the PL peak;[22] we thus chose a similar SPR range for GNBs and GNRs. As the PL QY is determined by the ratio between the emitted photons and absorbed photons, it is indispensable to obtain the absorption cross section. At the excitation of 532 nm along the long axis, the absorption efficiency is not much size-dependent both for GNBs and GNRs, as can be seen in Figure 5 and Supporting Information Figure S4. This is not unexpected because 532 nm is not close to the size-dependent longitudinal resonant wavelength of GNBs and GNRs.[33] In contrast, the total absorption is strongly dependent on the overall size of GNBs and GNRs as it is proportional to the volume.[36] Therefore, we have to obtain the precise volume value in order to deduce the PL QY from the PL intensity.

The geometric shape of the GNR and GNB is defined as in Supporting Information Figure S1 and Figure 1. The AFM technique was applied to estimating the value of the volume since it is very accurate for measuring the height of nanoparticles.[26]

At the beginning of the experiment, we scanned the selected GNB and GNR by AFM and obtained their morphology images as shown in the inset of Figure 6a and Supporting Information Figure S5a. From their cross section lines, the height *H* of the GNB and GNR can be acquired. For GNRs, $H = W$. In the case of GNBs, L/W was found in the range of 2.4−3.2 from TEM statistical results, suggesting that they are strongly elongated in our experiments. Depending on these TEM data, H/W was estimated to be in the range of 0.923−0.954. We set H/W to be 0.939 which is in the middle of the range. *W* can then be estimated after the height *H* of the GNB is measured by AFM. Given that the shape of the GNB is strongly elongated and thus the range of H/W is small, the estimation error for *W* and absorption cross section in this step is less than 4% and 8%, respectively. We scanned the height both

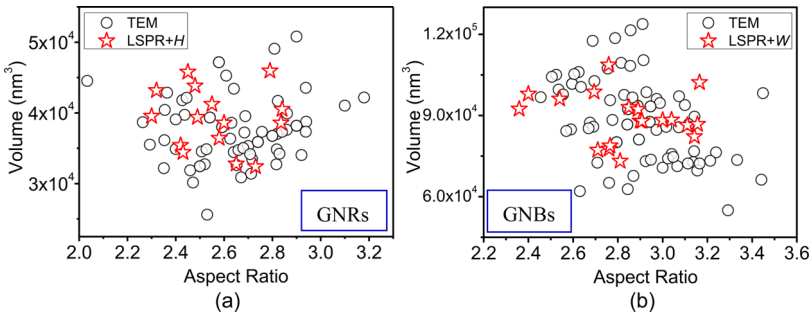

Figure 7. The effective volume of individual GNRs/GNBs estimated by combining PL and AFM measurements together with DDA simulations (red open stars) as a function of the aspect ratio. The TEM statistical results are represented by the black open circles. Each individual dot stands for one particle.

along the long axis and short axis, as shown by the dark solid and red dashed lines in Figure 6a. The difference is found to be less than 1 nm, confirming that the height measurement is very accurate by AFM. The slope of the cross section line along the long axis shown in Figure 6a is observed to be sharper at the right side which means that the left side of the monitored GNB is sitting on the substrate (refer to its top inset). Then we excited the target GNB and GNR by a CW laser (532 nm, 9 kW/cm^2) and collected their PL spectra as displayed in Figure 6b and Supporting Information Figure S5b (scattered line). As have been pointed out in Figure 3a, the PL spectrum follows closely with the scattering spectrum. Therefore, it can be utilized as a reference to calculate the extinction and absorption spectrum in the DDA simulation. When we combine the width of the GNB/GNR with the peak position in the absorption spectra, the length L and aspect ratio R can be determined by DDA. The solid line in Figure 6b and Supporting Information Figure S5b plots the simulated absorption spectrum. Please note that when we calculated the extinction and absorption spectrum, we have considered the difference between the spectrum of PL and scattering based on the experimental results shown in Figure 3a. On the basis of the obtained width W and the length L, the effective volume of the GNB and GNR can be calculated out. The red open stars in Figure 7a,b summarize the relationship between the aspect ratio and the effective volume for individual GNRs/GNBs.

Another direct way to estimate the effective volume of GNRs and GNBs is by TEM imaging. As we cannot correlate TEM measuring with optical characterization in our experiment, we made statistics analysis of the size data of GNRs and GNBs and plot them in Figure 7. It can be seen that all the volume value obtained by the above method is in the range of the TEM data statistical results, suggesting that the estimation is reliable.

On the basis of above analyses, we calculated the PL QY of single GNRs and GNBs by combining their absorption efficiency Q_{abs} calculated from DDA simulations with the obtained effective volume. In Figure 8a, b, we demonstrate the results for individual GNRs and GNBs as a function of the aspect ratio ranging from 2.3 to 3.2 and corresponding SPR from 590 to 740 nm. As can be observed, with an increase of the aspect ratio, there is a slight increase of the PL QY for both GNBs and GNRs in our investigation range. These results are similar to what have been observed for GNRs in another paper.[22] The statistically analyzed results shown in the caption of Figure 1 show that the averaged apex angle between the extended side edge lines of GNBs is increased from 29.2° to 33.2° with a decrease of the aspect ratio. Therefore, the slight increase of the PL QY with the aspect ratio for GNBs may be originated from the decrease of the apex angle. The more important result we observe here is that the PL QY of GNBs is doubled compared with that of GNRs in the similar SPR range. Given that the estimation error for the absorption cross section being less than 8%, it is convincing to conclude that the PL QY of GNBs is obviously higher than that of GNRs.

According to Fermi's golden rule, the spontaneous emission lifetime for a radiating dipole is dependent on the density of states (DOS). Controlling the field intensity can modulate the DOS and the radiative recombination rate between excited electrons and holes.[37] Thus, the emission quantum efficiency can be altered by the field intensity. As the lightning-rod effect is frequency-independent, we consider the field enhancement both at the excitation and emission wavelengths. Previously, Kou *et al.* calculated the distribution of the field intensity around the GNR and GNB along their symmetric cross sections.[38] Since both the volume and shape has a strong effect on the field distribution, the results along one certain cross section may not be able to comprehensively reflect its influence especially when the shape of the nanoparticle is complicated. We thus conducted three-dimensional calculations. As the field inside metallic nanoparticles obtained by DDA simulations is not reliable,[39] we use the variation trend of the field outside (0.5 nm away from the interface) the particle with the shape to reflect its inside trend by integrating the field intensity over the volume enclosing the GNR/GNB (with a thickness of 5 nm as shown in Figure 8d). This is

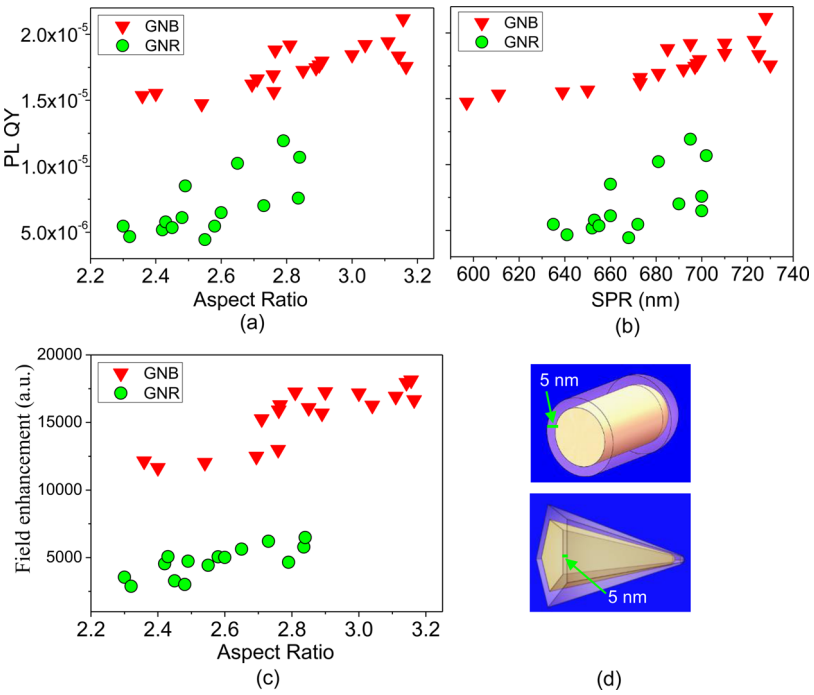

Figure 8. Photoluminescence quantum yield of individual GNRs (green filled circles) and GNBs (red filled triangles) as a function of (a) the aspect ratio and (b) plasmon resonance wavelength. Each individual dot represents one particle. (c) Normalized field intensity integrated over the volume surrounding the GNR/GNB (the part between the purple and golden surfaces with a thickness of 5 nm) as indicated in (d). (d) demonstrates the schematic diagram of the GNR/GNB, in which the left side shows the cross section along the short axis of the GNR/GNB.

reasonable because the field across interfaces is continuity. The geometrical parameters were taken from the experimental results. The results along the same cross sections of the GNR/GNB (with the largest and smallest aspect ratios in the experimental data) as in the ref 38 are shown in Supporting Information Figure S6. The similarity between them convinces the validity of our calculations. As the volume effect has been eliminated by taking into account of the absorption cross section in the experimental results, the integrated filed intensity in the calculation is normalized to the effective volume surrounding the GNR/GNB and plotted in Figure 8c. Please note here that all the field distributions demonstrated in our paper have been normalized to the incident and thus it can be called field enhancement. From Figure 8a–c, we can observe a consistent trend for the field intensity and PL QYs in a similar aspect ratio range. Therefore, we can ascribe the improved PL QYs of individual GNBs to the enhanced field intensity around them. However, as the stronger field intensity can enhance both the radiative decay rate of plasmon emissions and recombination rate of election-hole pairs, we cannot provide a conclusive emission mechanism in this paper.

CONCLUSIONS

In conclusion, based on single-particle measurements, we investigated the PL and scattering properties of individual GNBs under different excitation and detection polarizations. We found that the PL and scattering are spectrally overlapped and dominantly polarized along with the long axis of GNBs. Their absorption and emission dipoles are collinear. These results are analogous to those from the well-studied GNRs, suggesting that their emitting mechanisms are similar. Furthermore, by combining PL and AFM measurements together with DDA simulations, we introduced a new method to evaluate the geometric parameters of single GNBs and GNRs. TEM analysis results support its reliability. When we compare to the PL QY of individual GNRs, that for GNBs, which is in the similar SPR range, was found to be doubled. The calculation suggests that the higher PL QY is originated from the stronger field intensity integrated over the volume enclosing the GNB.

METHODS

Preparation of Gold Nanobipyramids and Gold Nanorods. The synthesis procedure for GNRs is described in the Supporting Information. GNBs were prepared chemically in aqueous solutions by a seed-mediated method as described in previous references.[28,29] All solutions were prepared freshly for each synthesis in deionized (DI) water. First, 20 mL of a solution of 0.125 mM $HAuCl_4$ and 0.25 mM sodium citrate was mixed followed by addition of 0.3 mL of 10 mM $NaBH_4$ solution at room temperature and stirring for 2 min. After the solution was kept at room temperature for at least 2 h for complete reaction, the color of the solution was dark pink and stable. Second,

0.5 mL of 10 mM $HAuCl_4$ and 10 mL of 100 mM cetyltrimethylammonium bromide (CTAB) were mixed with 0.1 mL of 10 mM silver nitrate to prepare the growth solution. Then, 0.2 mL of 1.0 M hydrochloric acid and 0.08 mL of 100 mM L-ascorbic acid were added into the solution orderly. Finally, the seed solution was added into the growth solution. The volume of the seed solution varied between 35 and 300 μL to synthesize different sizes of GNBs. These solutions were kept at 28 °C for several hours and their color changed gradually from almost clear to dark pink and remained.

AFM and Photoluminescence Measurement of Individual GNBs and GNRs. Two home-built systems demonstrated in Supporting Information Figure S2 were utilized to conduct measurements. The system shown in Supporting Information Figure S2a is based on an inverted fluorescence microscope combined with a DF scattering measurement function. It enables us to measure the luminescence and corresponding scattering properties of individual nanoparticles simultaneously. The details of this setup are described in our previous paper.[9] For PL measurements, the samples were excited by a diode-pumped solid-state 532 nm laser (CW, 9 kW/cm^2) that was directed through an oil immersion objective (100/0.6−1.3 NA Zeiss). A half-wave plate was inserted into the incident circuit to rotate the polarization of the excitation with respect to the laboratory reference system from 0° to 360° with a 10° increment. With a dichroic filter and a long pass filter to block the excitation light in the detection path, the PL spectra from individual GNBs and GNRs were collected by the same objective and detected using an electron multiplying charge-coupled device (EMCCD) camera. PL images were recorded with an intensified charge-coupled device (CCD) (Carl Zeiss) camera. A broad-band polarization analyzer was placed in the output optical path to examine the polarization characteristics of the PL, which were recorded consecutively as the analyzer was rotated at a step size of 10°. The dark-field scattering images and spectra were conducted on the same setup, with the dichroic and long pass filter removed. The white light generated by a halogen lamp was focused onto the sample by a condenser (NA = 0.7) and collected by the tunable oil immersion objective. Except for polarization measurements, the white light was randomly polarized. All the PL and scattering measurements were conducted at room temperature.

The system shown in Supporting Information Figure S2b consists of a home-built inverted fluorescence microscope combined with AFM. The combined setup is utilized to measure the PL properties of individual nanoparticles and their corresponding height H simultaneously. For detecting the height, we used a tapping mode in AFM with a scan rate of 0.5 Hz to record the signal and thus construct its topographic image. PL measuring is similar to the system shown in Supporting Information Figure S2a and the excitation power was also 9 kW/cm^2.

DDA Simulation. We performed extinction, absorption, scattering and field intensity calculations using the DDSCAT 7.1 code.[40,41] The particle was subdivided into N polarizable points located on a cubic lattice with an interdipole distance d. The particle volume is $V = Nd^3$. The effective volume of the particle can be represented by $V_{eff} = (4\pi r_{eff}^3)/3$, in which r_{eff} is defined as the radius of a sphere with a volume equal to that of the particle.

The dielectric function of gold was taken from the literature.[42] The grid size was chosen to be 0.5 nm to obtain convergent results. For GNRs, the ends are modeled as half spheres with the diameter the same as the rod. In the case of GNBs, the apexes are modeled as spherical caps with five cut facets. As the radius was found to be in the range of 2.7−3.4 nm by statically analyzed all the TEM results, we fixed it to be 3 nm to simplify the simulation. This estimation is reasonable because the variation of the radius in such a small range would not influence the absorption spectrum strongly.[39] The refractive index n of the surrounding medium in solutions was chosen to be 1.33, while that between air and the substrate was set to be 1.25.[22] All the filed distributions have been normalized to the incident.

As the field intensity decays rapidly from the surface of the metallic nanoparticles, we integrated the field intensity over the volume (with a thickness of 5 nm from the surface, refer to Figure 8d) surrounding the GNR/GNB. This calculation can provide more comprehensive information about the influence of the field intensity on the PL from nanoparticles. Considering the lightning-rod effect is frequency-independent, the integrated field intensity at the excitation and emission wavelengths are multiplied.[11]

Calculation of Photoluminescence Quantum Yield. The PL QY of individual GNBs and GNRs was calculated based on the measured PL spectrum and estimated effective volume. Specifically, it can be calculated according to the following equation:[22,33,43]

$$\Phi = \frac{N_{em}}{N_{abs}} = \frac{N_{signal}/\text{Det.Eff}}{\sigma_{abs} I/h\nu_{352}} = \frac{N_{signal}}{\text{Det.Eff}} \frac{h\nu_{352}}{\sigma_{abs} I}$$
$$= \frac{N_{signal}}{\text{Det.Eff}} \frac{h\nu_{352}}{Q_{abs}\pi r_{eff}^2 I}$$

where N_{em} and N_{abs} are the number of emitted and absorbed photons excited along their long axes. N_{signal} is the background-corrected signal intensity and I is the incident laser intensity. $\sigma_{abs} = Q_{abs}\pi r_{eff}^2$ is the absorption cross section and Q_{abs} is the absorption efficiency at a wavelength of 532 nm. Q_{abs} is obtained from the DDA simulation. r_{eff} is estimated by combining the AFM measurement, PL spectrum and DDA simulation. $h\nu_{532}$ represents the energy for a photon at the excitation wavelength of 532 nm. The detection efficiency, Det. Eff, was estimated to be 5‰ in our measurement.

Conflict of Interest: The authors declare no competing financial interest.

Acknowledgment. The authors acknowledge the financial support from the National Natural Science Foundation of China (Grant No. 61378082) and the Project of High-level Professionals in the Universities of Guangdong Province.

Supporting Information Available: Additional results. This material is available free of charge *via* the Internet at http://pubs.acs.org.

REFERENCES AND NOTES

1. Prasad, P. N. *Nanophotonics*; John Wiley & Sons, Inc.: New York, 2004.
2. Zijlstra, P.; Orrit, M. Single Metal Nanoparticles: Optical Detection, Spectroscopy and Applications. *Rep. Prog. Phys.* **2011**, *74*, 106401.
3. Raschke, G.; Kowarik, S.; Franzl, T.; Sonnichsen, C.; Klar, T. A.; Feldmann, J.; Nichtl, A.; Kurzinger, K. Biomolecular Recognition Based on Single Gold Nanoparticle Light Scattering. *Nano Lett.* **2003**, *3*, 935–938.
4. Anker, J. N.; Hall, W. P.; Lyandres, O.; Shah, N. C.; Zhao, J.; Van Duyne, R. P. Biosensing with Plasmonic Nanosensors. *Nat. Mater.* **2008**, *7*, 442–453.
5. Tcherniak, A.; Dominguez-Medina, S.; Chang, W. S.; Swanglap, P.; Slaughter, L. S.; Landes, C. F.; Link, S. One-Photon Plasmon Luminescence and Its Application to Correlation Spectroscopy as a Probe for Rotational and Translational Dynamics of Gold Nanorods. *J. Phys. Chem. C* **2011**, *115*, 15938–15949.
6. Wang, H. F.; Huff, T. B.; Zweifel, D. A.; He, W.; Low, P. S.; Wei, A.; Cheng, J. X. *In Vitro* and *in Vivo* Two Photon Luminescence Imaging of Single Gold Nanorods. *Proc. Natl. Acad. Sci. U.S.A.* **2005**, *102*, 15752–15756.
7. Durr, N. J.; Larson, T.; Smith, D. K.; Korgel, B. A.; Sokolov, K.; Ben-Yakar, A. Two-Photon Luminescence Imaging of Cancer Cells Using Molecularly Targeted Gold Nanorods. *Nano Lett.* **2007**, *7*, 941–945.
8. Wu, X.; Ming, T.; Wang, X.; Wang, P. N.; Wang, J. F.; Chen, J. Y. High-Photoluminescence-Yield Gold Nanocubes: For Cell Imaging and Photothermal Therapy. *ACS Nano* **2010**, *4*, 113–120.
9. Li, T.; Li, Q.; Xu, Y.; Chen, X. J.; Dai, Q. F.; Liu, H. Y.; Lan, S.; Tie, S. L.; Wu, L. J. Three-Dimensional Orientation Sensors by Defocused Imaging of Gold Nanorods through an Ordinary Wide-Field Microscope. *ACS Nano* **2012**, *6*, 1268–1277.
10. Mooradian, A. Photoluminescence of Metals. *Phys. Rev. Lett.* **1969**, *22*, 185–187.

11. Boyd, G. T.; Yu, Z. H.; Shen, Y. R. Photoinduced Luminescence from The Noble Metals and Its Enhancement on Roughened Surfaces. *Phys. Rev. B* **1986**, *33*, 7923–7936.
12. Mohamed, M. B.; Volkov, V.; Link, S.; El-Sayed, M. A. The 'Lightning' Gold Nanorods: Fluorescence Enhancement of Over a Million Compared to the Gold Metal. *Chem. Phys. Lett.* **2000**, *317*, 517–523.
13. Eustis, S.; El-Sayed, M. A. Aspect Ratio Dependence of the Enhanced Fluorescence Intensity of Gold Nanorods: Experimental and Simulation Study. *J. Phys. Chem. B* **2005**, *109*, 16350–16356.
14. Boyd, G. T.; Rasing, T.; Leite, J. R. R.; Shen, Y. R. Local-Field Enhancement on Rough Surfaces of Metals, Semimetals, and Semiconductors with The Use of Optical Second-Harmonic Generation. *Phys. Rev. B* **1984**, *30*, 519–526.
15. Dulkeith, E.; Niedereichholz, T.; Klar, T. A.; Feldmann, J.; von Plessen, G.; Gittins, D. I.; Mayya, K. S.; Caruso, F. Plasmon Emission in Photoexcited Gold Nanoparticles. *Phys. Rev. B* **2004**, *70*, 205424.
16. Wilcoxon, J. P.; Martin, J. E.; Parsapour, F.; Wiedenman, B.; Kelley, D. F. Photoluminescence from Nanosize Gold Clusters. *J. Chem. Phys.* **1998**, *108*, 9137–9143.
17. Nan, X. L.; Sims, P. A.; Xie, X. S. Organelle Tracking in a Living Cell with Microsecond Time Resolution and Nanometer Spatial Precision. *ChemPhysChem* **2008**, *9*, 707–712.
18. Lasne, D.; Blab, G. A.; Berciaud, S.; Heine, M.; Groc, L.; Choquet, D.; Cognet, L.; Lounis, B. Single Nanoparticle Photothermal Tracking (SNaPT) of 5-nm Gold Beads in Live Cells. *Biophys. J.* **2006**, *91*, 4598–4604.
19. Slaughter, L. S.; Wu, Y.; Willingham, B. A.; Nordlander, P.; Link, S. Effects of Symmetry Breaking and Conductive Contact on the Plasmon Coupling in Gold Nanorod Dimers. *ACS Nano* **2010**, *4*, 4657–4666.
20. Chang, W. S.; Ha, J. W.; Slaughter, L. S.; Link, S. Plasmonic Nanorod Absorbers as Orientation Sensors. *Proc. Natl. Acad. Sci. U.S.A.* **2010**, *107*, 2781–2786.
21. Imura, K.; Okamoto, H. Properties of Photoluminescence from Single Gold Nanorods Induced by Near-Field Two-Photon Excitation. *J. Phys. Chem. C* **2009**, *113*, 11756–11759.
22. Yorulmaz, M.; Khatua, S.; Zijlstra, P.; Gaiduk, A.; Orrit, M. Luminescence Quantum Yield of Single Gold Nanorods. *Nano Lett.* **2012**, *12*, 4385–4391.
23. Mayer, K. M.; Hao, F.; Lee, S.; Nordlander, P.; Hafner, J. H. A Single Molecule Immunoassay by Localized Surface Plasmon Resonance. *Nanotechnology* **2010**, *21*, 255503.
24. Eric, C. L. R.; Johan, G.; Idrissa, S.; Walter, R. C. S.; Pablo, G. E.; Treguer-Delapierre, M.; Charron, G.; Nordin, F.; Georges, L.; Jean, A. A Scheme for Detecting Every Single Target Molecule with Surface-Enhanced Raman Spectroscopy. *Nano Lett.* **2011**, *11*, 5013–5019.
25. Zhang, T. Y.; Shen, H. M.; Lu, G. W.; Liu, J.; He, Y. B.; Wang, Y. W.; Gong, Q. H. Single Bipyramid Plasmonic Antenna Orientation Determined by Direct Photoluminescence Pattern Imaging. *Adv. Opt. Mater.* **2013**, *1*, 335–342.
26. Markiewicz, P.; Goh, M. C. Simulation of Atomic Force Microscope Tip—Sample/Sample—Tip Reconstruction. *J. Vac. Sci. Technol., B* **1995**, *13*, 1115.
27. Viarbitskaya, S.; Teulle, A.; Marty, R.; Sharma, J.; Girard, C.; Arbouet, A.; Dujardin, E. Tailoring and Imaging the Plasmonic Local Density of States in Crystalline Nanoprisms. *Nat. Mater.* **2013**, *12*, 426–432.
28. Liu, M. Z.; Guyot-Sionnest, P. J. Mechanism of Silver(I)-Assisted Growth of Gold Nanorods and Bipyramids. *J. Phys. Chem. B* **2005**, *109*, 22192–22200.
29. Lee, S.; Mayer, K. M.; Hafner, J. H. Improved Localized Surface Plasmon Resonance Immunoassay with Gold Bipyramid Substrates. *Anal. Chem.* **2009**, *81*, 4450–4455.
30. Jana, N. R.; Gearheart, L.; Murphy, C. J. Wet Chemical Synthesis of High Aspect Ratio Cylindrical Gold Nanorods. *J. Phys. Chem. B* **2001**, *105*, 4065–4067.
31. Zhou, X. C.; Andoy, N. M.; Liu, G. K.; Choudhary, E.; Han, K. S.; Shen, H.; Chen, P. Quantitative Super-Resolution Imaging Uncovers Reactivity Patterns on Single Nanocatalysts. *Nat. Nanotechnol.* **2012**, *7*, 237–241.
32. Novo, C.; Funston, A. M.; Mulvaney, P. Direct Observation of Chemical Reactions on Single Gold Nanocrystals Using Surface Plasmon Spectroscopy. *Nat. Nanotechnol.* **2008**, *3*, 598–602.
33. Fang, Y.; Chang, W. S.; Willingham, B.; Swanglap, P.; Dominguez-Medina, S.; Link, S. Plasmon Emission Quantum Yield of Single Gold Nanorods as a Function of Aspect Ratio. *ACS Nano* **2012**, *6*, 7177–7184.
34. Hu, H.; Duan, H.; Yang, J. K.; Shen, Z. X. Plasmon-Modulated Photoluminescence of Individual Gold Nanostructures. *ACS Nano* **2012**, *6*, 10147–10155.
35. Lin, C. A. J.; Yang, T. Y.; Lee, C. H.; Huang, S. H.; Sperling, R. A.; Zanella, M.; Li, J. K.; Shen, J. L.; Wang, H. H.; Yeh, H. I.; et al. Synthesis, Characterization, and Bioconjugation of Fluorescent Gold Nanoclusters toward Biological Labeling Applications. *ACS Nano* **2009**, *3*, 395–401.
36. Gaiduk, A.; Yorulmaz, M.; Orrit, M. Correlated Absorption and Photoluminescence of Single Gold Nanoparticles. *ChemPhysChem* **2011**, *12*, 1536–1541.
37. Neupane, B.; Zhao, L. Y.; Wang, G. F. Up-Conversion Luminescence of Gold Nanospheres When Excited at Nonsurface Plasmon Resonance Wavelength by a Continuous Wave Laser. *Nano Lett.* **2013**, *13*, 4087–4092.
38. Kou, X. S.; Ni, W. H.; Tsung, C. K.; Chan, K.; Lin, H. Q.; Stucky, G. D.; Wang, J. F. Growth of Gold Bipyramids with Improved Yield and Their Curvature-Directed Oxidation. *Small* **2007**, *3*, 2103–2113.
39. Liu, M. Z.; Guyot-Sionnest, P.; Lee, T. W.; Gray, S. K. Optical Properties of Rodlike and Bipyramidal Gold Nanoparticles from Three-Dimensional Computations. *Phys. Rev. B* **2007**, *76*, 235428.
40. Yurkin, M. A.; Maltsev, V. P.; Hoekstra, A. G. The Discrete Dipole Approximation: An Overview and Recent Developments. *J. Quant. Spectrosc. Radiat. Transfer* **2007**, *106*, 546–557.
41. Draine, B. T.; Flatau, P. J. User Guide for the Discrete Dipole Approximation Code DDSCAT 7.1, 2010. Available from: http://arXiv.org/abs/1002.1505v1.
42. The information on the refractive indices of materials is available on the website http://refractiveindex.info/.
43. Gaiduk, A.; Ruijgrok, P. V.; Yorulmaz, M.; Orrit, M. Making Gold Nanoparticles Fluorescent for Simultaneous Absorption and Fluorescence Detection on the Single Particle Level. *Phys. Chem. Chem. Phys.* **2011**, *13*, 149–153.